HHS Public Access

Author manuscript

Transl Res. Author manuscript; available in PMC 2018 March 01.

Published in final edited form as:

Transl Res. 2017 March ; 181: 1–14. doi:10.1016/j.trsl.2016.09.006.

Advances in Imaging Approaches to Fracture Risk Evaluation

Mary Kate Manhard[1,2], **Jeffry S. Nyman**[1,2,3,4,5], and **Mark D. Does**[1,2,6,7]

[1]Biomedical Engineering, Vanderbilt University, Nashville, TN

[2]Vanderbilt University Institute of Imaging Science, Nashville, TN

[3]Orthopaedic Surgery and Rehabilitation, Vanderbilt University, Nashville, TN

[4]Tennessee Valley Healthcare System, Department of Veterans Affairs, Nashville, TN

[5]Center for Bone Biology, Vanderbilt University Medical Center, Nashville, TN

[6]Radiology and Radiological Sciences, Vanderbilt University, Nashville, TN

[7]Electrical Engineering, Vanderbilt University, Nashville, TN

Abstract

Fragility fractures are a growing problem worldwide, and current methods for diagnosing osteoporosis do not always identify individuals who require treatment to prevent a fracture and may misidentify those not a risk. Traditionally, fracture risk is assessed using dual-energy X-ray absorptiometry, which provides measurements of areal bone mineral density (BMD) at sites prone to fracture. Recent advances in imaging show promise in adding new information that could improve the prediction of fracture risk in the clinic. As reviewed herein, advances in quantitative computed tomography (QCT) predict hip and vertebral body strength; high resolution HR-peripheral QCT (HR-pQCT) and micro-magnetic resonance imaging (μMRI) assess the micro-architecture of trabecular bone; quantitative ultrasound (QUS) measures the modulus or tissue stiffness of cortical bone; and quantitative ultra-short echo time MRI methods quantify the concentrations of bound water and pore water in cortical bone, which reflect a variety of mechanical properties of bone. Each of these technologies provides unique characteristics of bone and may improve fracture risk diagnoses and reduce prevalence of fractures by helping to guide treatment decisions.

Introduction

Bone fractures are a widespread problem that affect over 75 million people in the world, with more than 2.3 million osteoporotic fractures per year globally (1, 2). Over a lifetime, the risk of a fracture is around 40% for women in developed countries (3). The costs associated with bone fractures were estimated to be $19 billion in 2005 in the United States

Correspondence to: Mark D. Does, 1161 21 Ave S, AA-1105 MCN, Nashville, TN 37232-2310, mark.does@vanderbilt.edu.

alone, and are projected to increase by 50% by the year 2025 (4). In the EU, costs in 2010 were estimated to be €37 billion, and are expected to increase by 25% in 2025 (1). An increase in fracture risk occurs with aging for both women and men (4, 2). Fractures are a large problem with certain diseases and conditions, such as post-menopausal women and diabetes. Diabetes, in particular, has a rapidly increasing prevalence (5), leading to even higher costs and an increasing need for comprehensive clinical procedures to accurately measure and diagnose fracture risk.

The most common imaging parameter used to diagnose high fracture risk is low bone mineral density (BMD) assessed by dual energy X-ray absorptiometry (DXA) of the hip, spine, and distal radius. Examples of DXA images acquired in the radius and the hip are shown in Figure 1. DXA measures the transmission of X-ray beams through tissue at two different mean photon energies. The difference in dependence of X-ray attenuation on photon energy between bone mineral and soft tissues then allows for an estimate of BMD (6). Because DXA uses 2D projection images, the resulting BMD values are areal estimates, computed in units of mineral mass per image pixel area. In clinical practice, however, DXA BMD is typically evaluated as a T-score (tabulated over a standard region of interest), defined as an individual's BMD relative to the standard deviation of BMD values of a young healthy population of the same ethnicity and sex (7). The World Health Organization has defined osteoporosis as having a T-score lower than −2.5 or having a previous fragility fracture, and osteopenia is defined as having a T-score between −1 and −2.5.

DXA is a fast, inexpensive, and well-studied method that has very low radiation dose (5–20 μSv), but it also has many limitations. Areal BMD varies significantly based on anatomical structure, so the results are biased by bone size and orientation. Degenerative disc disease or aortic calcifications can lead to an increased apparent BMD and falsely lower apparent fracture risk (8, 9), while other imaging artifacts arising from excess soft tissue in obese patients or prosthetic implants in the background can also alter DXA results. In addition, DXA does not fully explain the increase in fracture risk with age (10) or diabetes (11). Moreover, in a study of nearly 150,000 post-menopausal women (50 to 104 yo), 82% of those that reported a fracture within one year had a baseline T-score greater than −2.5 (DXA at peripheral sites, namely heel, finger, or forearm) (12).

To overcome some of the limitations of DXA, it is now standard of care to consider additional risk factors in the diagnosis and treatment of osteoporosis. This is often done using algorithms that incorporate known risk factors, such as The World Health Organization's Fracture Risk Algorithm (FRAX) tool (13). This online tool calculates the 10-year probability of a major osteoporotic fracture and of a hip fracture based on relevant risk factors (e.g., age, sex, history of fracture, smoking status, alcohol consumption, and various diseases associated with high fracture) with or without hip BMD. The FRAX model is widely used in the clinic and is continuing to be expanded to include more countries. However, FRAX does not include all ethnicities or diseases, for instance type-2 diabetes, and is only designed to help guide clinical decisions. Other algorithms, such as Garvan and QFracture, have also been introduced as an alternatve to FRAX. The Garvan algorithm (14) was developed in Australia, includes the probability of suffering a fracture within both 5 and 10 years, and uses the history and frequency of previous fractures and falls. However, it does

not include other risk factors and has only been tested on Australian and Canadian populations. The QFracture method (15) was developed in the United Kingdom and includes more risk factors than FRAX, such as various diseases, history of falls, and a 5 point scale for history of smoking and alcohol use. However, it does not include previous fractures in the model, and is limited to studies in the UK. In addition to the risk factor models, the trabecular bone score (TBS) is a gray-level texture measure that is derived from experimental variograms of DXA images of the lumbar spine. TBS is an indirect index of trabecular architecture, and has shown promise in adding to the predictive power of DXA (16). While both TBS and risk factor algorithms are useful tools, the primary limitation of these measures is that they lack additional information about the composition of the bone itself (17, 18).

Changes in both cortical and trabecular bone alter bone strength. With aging, there can be a thinning of the cortices, due to endosteal resorption, that leads to an increase in fracture risk (19). Aging can also lead to deterioration of the trabecular architecture (e.g., fenestrations of the trabeculae lowering the connectivity), thereby weakening the bone (20). Because bone loss usually begins in trabecular bone, clinicians are often interested in looking at trabecular bone measures to detect early changes in bone quality. Some more recent imaging methods have aimed to look at properties beyond areal BMD from DXA (21, 22).

Regardless of type, the bone tissue is comprised of three principal components: i) mineral (primarily crystals of calcium phosphate with carbonate and hydroxyl substitutions), ii) organic matrix (primarily type 1 collagen, non-collagenous proteins, and lipids), and iii) water (existing in porous spaces and bound to the matrix). The mineral component imparts strength and stiffness, and is the component of bone to which DXA is sensitive. However, the mineral component of bone alone is brittle; the plasticity or ductility of the bone comes from the hydrated organic matrix. During plastic deformation (i.e., post-yield strain), energy is dissipated until the bone fractures(19, 23). Along with bone structure, both the strength and plasticity of the bone tissue contribute to fracture resistance. Though increases in fracture risk are usually attributed to a decrease in BMD, changes in collagen organization or condition also affect fracture risk. For example, as a person ages, the collagen integrity of their bones decreases which results in increased brittleness of the bone (24, 25), leading to a significant increase in fracture risk. A major challenge in bone imaging is finding useful surrogates that are sensitive to bone brittleness.

This paper reviews additional imaging techniques that probe properties of bone that have the potential to help better diagnose fracture risk in clinical settings. The methods discussed are quantitative computed tomography (QCT) including high resolution peripheral QCT (HR-pQCT), quantitative ultrasound (QUS), micro magnetic resonance imaging (μMRI), and other quantitative MRI methods that provide information about the composition of the tissue. QCT methods provide 3D bone structure and volumetric BMD, which in-turn can also support the use of numerical methods to predict bone strength. High resolution HR-peripheral QCT (HR-pQCT) and micro-magnetic resonance imaging (μMRI) both assess the micro-architecture of trabecular bone. HR-pQCT also provides volumetric BMD, but at the cost of radiation exposure; μMRI has no ionizing radiation, allowing for repeated measurements, but has lower resolution and does not report BMD. Both HR-pQCT and

μMRI have also been used in combination with μFEA to help improve bone strength predictions. QUS estimates of bone quality based on the ultrasound wave characteristics through bone tissue. Quantitative MRI methods can assess 3D bone structure, bone marrow fat content, and cortical bone water compartments including bound water and pore water components.

QCT and HR-pQCT

Quantitative computed tomography (QCT) uses conventional CT imaging applied in the lumbar vertebrae and proximal femur, concurrently with phantoms with known volumetric BMD values to convert image contrast into quantitative measures of volumetric BMD (mineral mass per image voxel volume) (26, 27, 28). More recently, opportunistic CT evaluations have been used to determine fracture risk (29, 30), in which CT scans acquired for reasons unrelated to osteoporosis are evaluated for low volumetric BMD in the spine or proximal femur. However, without a phantom, the scan is not quantitative, so this approach is only possible if the CT scanner is stable and calibrated regularly to ensure correct scaling of the intensity of the CT scans to Hounsfield units, which can be converted to BMD (29, 31, 30).

As a three dimensional measurement, QCT resolves whole bone structure and shape, but does not provide the resolution necessary to resolve trabeculae. Nonetheless, QCT can distinguish high volumetric BMD in cortical bone from low mean volumetric BMD in trabecular bone, and such measures of mean trabecular BMD in the proximal femur have been shown to discriminate between patients with and without hip fractures (32, 33, 34). QCT-derived volumetric BMD has also been shown to discriminate between patients with vertebral fractures and those with no fractures (35, 36, 37). In addition to volumetric BMD, measures such as cross sectional moment of inertia and cortical bone thickness can be determined. These measures have been shown to report on whole bone mechanical properties, as determined from tests on cadaveric bones (38, 33, 9, 34).

QCT-based finite element analysis (FEA) extends interpretations of QCT to incorporate whole bone structure (Figure 2). This computational approach for bone strength estimation has been reviewed in recent years (39, 40, 41) but a brief summary is given here. The voxels from a CT scan are used to define the finite elements that facilitate the numerical solution to the partial differential equations relating stress to the forces acting on bone (maintaining equilibrium) and relating strain to displacement (deformation of the bone). Each element is assigned material properties that define the stress-strain relationship or constitutive behavior of the bone tissue. These properties are typically based on empirical relationships between the apparent BMD and such elastic properties as modulus and yield strength. Boundary conditions simulating the forces experienced by a given bone in physiological conditions are applied, and a 3D mesh of coupled equations are solved numerically to estimate the stress and strain distribution in every element. This computation can be done using either linear or nonlinear models. Unlike linear models, nonlinear models allow plastic deformation to occur, but can require substantial computational time and memory to solve. A bone is considered to fail when it meets a certain fracture criteria such as exceeding an overall strain limit, or when a large enough volume of voxels exceeds an ultimate stress limit. Ex vivo

studies have shown strong correlations between FEA predicted strength and experimentally measured strength of the hip (42) and of the vertebra (43). Cross-sectional studies of QCT-based FEA have shown the ability to discriminate between fracture and non-fracture cases (44, 45, 46), and may be able to predict fracture better than BMD alone (43).

While QCT reports on the same mineral component of bone as DXA, it measures volumetric BMD, can be applied to both cortical and trabecular bone, and predicts whole bone strength. As a volumetric measure, QCT does not depend on the relative soft tissue attenuation, so it does not have the same issues as DXA with high attenuation in obese patients, or contamination from degenerative changes which can falsely increase areal BMD. QCT also allows for assessment of structural properties about the cortical bone size and shape.

Unlike QCT, high-resolution, peripheral QCT (HR-pQCT) can assess trabecular architecture and cortical porosity while also measuring volumetric BMD. HR-pQCT uses a dedicated imaging system for extremities at to achieve high resolution (80 μm isotropic) images of the distal tibia and/or distal radius. These systems provide both volumetric BMD and direct visualization of trabecular and cortical bone architecture, and an example of typical images in the distal radius can be seen in Figure 3. Cortical bone can be analyzed to assess parameters such as cortical thickness (Ct.Th), cortical porosity (Ct.Po) and cortical pore volume (Ct.Po.V). In trabecular bone, standard analysis includes quantifying structural properties of trabecular bone, such as bone volume fraction (BV/TV), which is derived from trabecular BMD (Tb.BMD), average number of trabeculae (Tb.N), average trabecular thickness (Tb.Th), and average trabecular separation (Tb.Sp) (47). Other trabecular properties have been explored as well, such as the connectivity (48), anisotropy (49), and structural model index (50), or individual trabecula segmentation (ITS) (51). The ITS software assesses contributions of plate and rod like structures in trabecular bone, such as ratio of rod to plate elements, orientation, plate and rod volume fractions and densities, and average size of plates and rods.

In comparison to DXA, HR-pQCT offers advantages in detecting early changes in trabecular bone in longitudinal studies in children (52) and transplant patients (53). Other examples of the utility of HR-pQCT include measurement of significant differences in trabecular architecture between post-menopausal women with and without history of fragility fractures (20, 54, 55), as well as differences in cortical porosity (56). Cortical pore volume (Ct.Po.V) was also found to be significantly higher in the tibia and radius of diabetic subjects (57). Following a period of disuse, it was found that detectable changes of the distal tibia microstructural properties occur, and recover when returning to normal weight bearing activity (58).

The isotropic voxels in a HR-pQCT image can be directly converted to elements for FEA, termed μFEA. Whereas the mesh of the bone is homogenized in QCT-FEA, the mesh in μFEA resolves bone from marrow spaces or pores. Linear μFEA can predict mechanical properties of the bone, such as the stiffness and strength (42, 59, 43), and have been shown to report on age and sex related differences (20, 60), to discriminate between fracture and non-fracture cases (61, 62, 63, 64), and to assess the severity of fractures (65, 66). μFEA has also shown potential for quantifying bone healing following a fracture (67, 68). Non-linear

μFEA models have also been used to estimate post-yield parameters such as toughness (69). Because the finite element models are generated from axial scans of select regions of distal sites, the boundary conditions in μFEA do not necessarily simulate the loads that occur during a fall.

While QCT and HR-pQCT both have the ability to gain information about fracture risk, these methods have some limitations. QCT is more expensive than DXA, and central QCT has a high radiation dose, so measurements cannot be repeated frequently. Therefore, QCT is only advised in specific cases such as with obese subjects or advanced degenerative disease, and for monitoring metabolic changes in trabecular bone. HR-pQCT has a low radiation dose because radiosensitive organs are not close to the area of the scan (70), but is limited to the extremities, and is sensitive to signal contamination from motion or beam hardening. Also, like DXA, neither QCT nor HR-pQCT are sensitive to changes in the collagen matrix of bone. Both QCT and HR-pQCT are useful for finding more specific information about bone quality than DXA, but with the extra cost and radiation dose, they have not replaced DXA as a screening tool.

Quantitative Ultrasound

Unlike CT methods, quantitative ultrasound (QUS) is a low-cost method that is widely available. QUS measures both velocity and amplitude properties of ultrasound waves through bone tissue (71). The velocity of the measured waves, speed of sound (SoS), and broadband ultrasound attenuation (BUA) are the most commonly used measures to assess bone tissue, as well as values calculated from a combination of these two, the stiffness index (SI) and the quantitative ultrasound index (QUI) (72). These quantitative measures have been shown to reflect elastic modulus and compressive strength of the bone tissue (73). QUS is most often performed in the calcaneus of the heel, which is of particular interest because it is comprised primarily of trabecular bone, where bone loss usually begins, and easily accessible for a QUS measurement.

While calcaneous QUS has shown moderate correlations with BMD from DXA (71, 74), there has been a growing amount of research showing that QUS measures are an independent risk factor of fracture (75, 76, 77, 78). Additionally, QUS measures have shown differences between subjects with fractures and subjects without fractures in many studies (79, 80, 75, 77, 78). It has also shown some association with proximal hip fractures (81), and tends to be a better predictor of hip fractures than spine fractures (82). QUS has similar sensitivity as DXA, but lower specificity, and has been approved to be used to identify those in a low risk population where no further screening may be necessary (83, 82).

QUS is portable, inexpensive, has no ionizing radiation, and can be used in low resource settings where DXA is not available. While the amount of evidence for QUS as an independent marker of fracture risk is increasing, it is still not well standardized in the clinic, especially compared to DXA (80, 82). QUS results are also dependent on the devices, operators, anatomical locations, and positioning of the bone and ultrasound transducer. Clinically, it is not currently a recommended method for diagnosing osteoporosis or guiding treatment decisions (84, 80) though more recently it has been suggested as a screening tool

for fracture risk assessment (83, 82). While it offers a radiation-free method of assessing bone, the efficacy of the methods need to be improved and further studied before it is a clinically viable tool (80, 85).

μMRI

Micro-MRI, or μMRI, evaluates both cortical and trabecular bone properties, such as cortical thickness and trabecular bone microarchitecture (86, 87, 88, 89), and performs similarly to HR-pQCT (90). Several pulse sequences have been used for high resolution structural imaging of bone, including spoiled gradient echo (91, 92), balanced steady state free precession (b-SSFP) (93, 94), and fast large spin echo (FLASE) (95, 96, 97). These pulse sequences all allow images to be acquired at a relatively high resolution (100–200μm in plane resolution). Unlike gradient echo or b-SSFP, spin echo methods such as FLASE are less sensitive to off resonance effects that can cause distortions in the trabecular architecture. However, spin echo sequences have a longer minimum acquisition time because the TR required is much longer (94). μMRI of bone is usually acquired at extremities such as the distal tibia or distal radius, but it has also been applied at the proximal femur (98, 99, 100), as shown in Figure 4.

Similar structural and architectural measurements as HR-pQCT can be derived from μMRI images (90). These measures of bone derived from μMRI have been shown to report on fracture risk. For example, many studies assessing achitectural properties in the distal radius have shown differences between fracture and non-fracture cases in the vertebrae (101, 102, 54), and other studies have shown changes in properties in response to drug treatment (103, 92, 104, 105). Recently, μMRI has been used with machine learning to improve the accuracy of discriminating between fracture and non-fracture cases (106). μMRI can also be used with μFEA to predict mechanical properties from structure (107, 108). For example, in renal transplant patients, μFEA showed significantly lower mechanical properties after transplantation (109), even when structural properties did not change significantly.

While μMRI probes similar characteristics of bone as HR-pQCT, μMRI has an advantage because it does not involve ionizing radiation, which enables repeated scans over a short time span and application to the proximal femur (98, 110, 111, 100). However, μMRI does not report on BMD, has lower spatial resolution, and is more expensive than HR-pQCT. Also, current μMRI methods are sensitive to magnetic susceptibility artifacts which can change the apparent size of trabeculae(94, 112), and motion artifacts due to the long scan times (113, 114). Overall, use of μMRI in the clinic is limited by resources and cost, but it has the potential to greatly add to the ability to predict fracture risk.

Other Quantitative MRI Methods

The imaging measurements of bone quality discussed thus far are only sensitive to the mineral composition of bone. While imaging the mineral component allows for measures of BMD as well as many structural changes that relate to bone strength, other components of bone such as the collagen content and the fat content can report on fracture resistance. Quantitative MR measures are sensitive to water and fat in the bone, including bone marrow

fat and collagen-bound water in cortical bone. It has been shown that there is a relationship between marrow fat content and fracture risk (115), because the adiposity of marrow is related to bone metabolism (116). Vertebral marrow fat fraction increases with age (117), as does the portions of saturated, monosaturated, and polyunsaturated fat (118). Generally, greater proportions of saturated marrow lipids are associated with increased fracture risk (119) and with lower DXA BMD (120).

MR spectroscopy (MRS) measures signal from a volume of tissue and then uses spectral analysis to determine the molecular sources of the signal—the signal amplitude at particular frequencies are related to the volume of a particular chemical components in the tissue. In particular, MRS of bone marrow can measure both the volume fraction of fat and the relative amounts of unsaturated and saturated fats (121), and has shown good reproducibility in the vertebrae (122, 123). Several MRS studies have shown a significant association between marrow fat fraction and prevalence of fractures (124, 118, 123, 125). MRS has also found altered bone marrow fat composition in type-2 diabetes cases, (126, 127, 125), where DXA tends to give higher BMD levels despite the increase in fracture risk. MRS has the advantage of being widely available on clinical MR systems, so it is relatively straightforward to implement.

In addition to the water and fat in marrow, MRI can probe both the water bound to the organic matrix (bound water) and the water residing in the pore space (pore water) of cortical bone. MRI images of cortical bone water in the tibia are shown in Figure 5. In cortical bone, the proton signal from different components can be distinguished by transverse relaxation time constant (T_2) (128, 129, 130). The collagen protons make up the pool with the shortest relaxation times ($T_2 < 100$ μs); the water bound to the collagen matrix of cortical bone has a relatively short T_2, 100 to 1000 μs; and the water in the pore spaces of cortical bone span wide range of T_2 values from 1 ms to 1 s, reflecting the wide range of pore sizes (131).

In conventional MRI scans, the echo time (TE) is longer than the T_2 of most of the bone water signal, so little or no bone signal can be seen in the image. However, imaging sequences such as ultra-short echo time (UTE) (132), water and fat suppressed projection imaging (WASPI) (133), zero echo time (ZTE) (134), and SWeep Imaging with Fourier Transform (SWIFT) (135) can reach effective echo times of 100 μs or less, permitting measurement of the bound and pore water signals, in particular. Most in vivo studies to date have used UTE (136, 137, 138, 139, 140, 141, 142, 143, 144), which is relatively easy to implement on clinical MRI systems. UTE imaging achieves a short TE by starting signal acquisition immediately following the radio-frequency excitation (and a short delay for switching the electronics from transmit to receive mode). Data are acquired while the read-out gradient ramps from zero, which means that k-space is sampled radially from the center and no delay is necessary for a phase-encoding or read-preparation gradient pulses. This also means that there is no time for a slice-select refocussing gradient pulse, so UTE requires either a 3D acquisition using non-selective excitation pulses or special slice-selective pulses that do not require gradient refocussing (discussed below). Naturally, UTE is not amenable to spin echo acquisition, so the signal amplitude as a function of TE depends on T_2^* not T_2.

Early UTE studies of cortical bone characterized total signal, but an NMR relaxometry study of cadaver bone samples demonstrated that the bound and pore water signal amplitudes change in opposite direction with change in bone mechanical properties (145, 146). Thus, UTE MRI methods that best predict fracture risk should robustly distinguish and quantitatively measure bound- and pore-water concentrations in cortical bone. An overview of methods developed for this purpose was recently presented in Seifert et al (147) and is briefly highlighted below.

One approach is to distinguish the bound and pore water signals by T_2^* rather than T_2 weighting. In the simplest form, two UTE images are acquired, one at the shortest achievable TE and one with a sufficiently long TE such that only pore water signal remains. A ratio of these two image intensities has been called the porosity index and corresponds well with the pore water fraction as well as μCT measures of porosity (144). A similar measure of relative amplitudes of bound and pore water through non-linear regression of intensities from several images with different effective TEs has also been implemented (148, 137, 149, 150) and has shown good correlations with mechanical properties of bone (141). These T_2^* based approaches are essentially equivalent to early non-localized studies of bone samples at low magnetic field (151); however, line broadening will tend to result in an overlap of bound and pore water signal T_2^* values making these approaches less effective at higher magnetic fields (152, 153, 154).

Alternatively, bound- and pore-water UTE MRI methods that discriminate bound and pore water signals based on T_2 (not T_2^*) using adiabatic RF pulses was proposed by Horch et al. (152) and later translated (155), validated (143), and shown to report on various mechanical properties of bone, including toughness (156). This approach is an extension of earlier UTE methods that used adiabatic RF pulses to suppress long T_2 signals from tissues such as muscle and bone marrow to enhance visibility of tissues with short T_2 signals, such as bone (157, 140, 158). Specifically, the adiabatic inversion recovery (AIR) method, for bound water imaging, uses an adiabatic full passage pulse followed by an appropriate delay to invert and null pore water magnetization while the bound water magnetization recovers from zero to near full amplitude. Similarly, two consecutive adiabatic full passage pulses will drive the bound water magnetization to zero while rotating pore water magnetization through 360, leaving it essentially unaffected. This approach is referred to as the Double Adiabatic Full Passage (DAFP) method and is used to image pore water. Both of these methods, similar to some previous and subsequent UTE studies of bone, use a reference marker with a known proton concentration in the imaging field of view in order to convert image intensity into a measure in absolute units of concentration.(139, 140, 159, 155). Representative bound and pore water concentration maps from in vivo acquisitions in the tibia and radius are shown in Figure 6.

While these quantitative UTE MRI methods are advantageous because they are sensitive to different components of bone than the other imaging methods discussed in this article, they have limited resolution and have only been applied in vivo in the radius and tibia. Also, MRI is expensive and can result in relatively long scan times compared to X-ray based methods. Using 2D UTE rather than 3D UTE can dramatically reduce scan times, but 2D UTE is

known to be highly sensitive to the performance of the magnetic field gradients (136, 160, 161). Recent technical developments in gradient waveform optimization (162) applied to 2D UTE have demonstrated the potential for quantitative bound and pore water imaging in the tibia in <1 min of scan time (163). This 2D UTE method has the potential to be applied in the femoral neck, where most traumatic fractures occur, though cortical bone in the femoral neck is thin, and these MRI methods need more development to be applicable in such areas. Beyond just the development of 2D UTE methods, continued developments and evaluations in clinical subjects are necessary to to determine the ultimate utility of quantitative UTE MRI.

Conclusion

A summary of the imaging methods discussed in this article are shown in Table 1. These emerging imaging methods have the potential to provide better fracture risk assessment than current clinical techniques. HR-pQCT and μMRI can help by providing more information on bone structure, particularly in trabecular bone microarchitecture. QUS offers information about the quality of bone at low cost. MRI methods for quantifying fat could also help to independently characterize fracture risk, especially in diabetic patients. Methods for imaging cortical bone using MRI can probe new information about the material properties of the bone, since they are sensitive to the bound and pore water components rather than the mineral component. To date, the evidence for the efficacy of the imaging methods to accurately assess fracture risk come from case-control studies. Moving forward, longitudinal, prospective studies are necessary to determine at what thresholds the measurements from advanced imaging techniques indicate when a patient requires fracture prevention therapy. Future work should refine these imaging methods to further enhance their sensitivity to fracture resistance of an indivdidual's bone.. The non-ionizing radiation methods are also well suited for longitudinal studies, which could help monitor disease progression over time, thereby assisting clinicians in deciding when an intervention is needed or when a drug treatment can be stopped. Imaging methods could also be used with personalized drug therapies to better prevent fractures or evaluate disease state. Newer imaging methods may also improve monitoring of the fracture healing process. In conclusion, developing new imaging methods to evaluate bone fracture risk could yield better and safer methods for treatment planning in cases of osteoporosis, diabetes, and other diseases associated with increased fracture risk, to ultimately reduce fragility fractures in patients.

Acknowledgments

The authors acknowledge funding from the NIH (R01EB014308, R01AR063157, S10RR027631) and internal funds from Vanderbilt University and the Vanderbilt University Medical Center. The authors have read the journal's policy on disclosure of potential conflicts of interest and have no financial or personal relationships that could potentially be perceived as influencing the described research. All authors have read the journal's authorship agreement and that the manuscript has been reviewed by and approved by all named authors.

Abbreviations

DXA dual energy x-ray absorptiometry

BMD	bone mineral density
FRAX	fracture risk algorithm
HR-pQCT	high resolution peripheral quantitative computed tomography
QUS	quantitative ultrasound
SoS	speed of sound
BUA	broadband ultrasound attenuation
SI	stiffness index
QUI	quantitative ultrasound index
NMR	nuclear magnetic resonance
MRI	magnetic resonance imaging
MRS	magnetic resonance spectroscopy
UTE	ultrashort echo time
DAFP	double adiabatic full passage
AIR	adiabatic inversion recovery

References

1. Hernlund E, Svedbom A, Ivergård M, Compston J, Cooper C, Stenmark J, McCloskey E, Jonsson B, Kanis J. Osteoporosis in the European Union: medical management, epidemiology and economic burden. Arch Osteoporos. 2013:8.
2. Wright NC, Looker AC, Saag KG, Curtis JR, Delzell ES, Randall S, DawsonHughes B. The Recent Prevalence of Osteoporosis and Low Bone Mass in the United States Based on Bone Mineral Density at the Femoral Neck or Lumbar Spine. J Bone Miner Res. 2014; 29:2520–2526. [PubMed: 24771492]
3. Organization WH. Technical report. World Health Organization; Brussels, Belgium: 2004. WHO scientific group on the assessment of osteoporosis at primary health care level.
4. Burge R, DawsonHughes B, Solomon DH, Wong JB, King A, Tosteson A. Incidence and Economic Burden of Osteoporosis-Related Fractures in the United States, 2005 to 2025. J Bone Miner Res. 2007; 22:465–475. [PubMed: 17144789]
5. Wild S, Roglic G, Green A, Sicree R, King H. Global prevalence of diabetes: estimates for the year 2000 and projections for 2030. Diabetes Care. 2004; 27:1047–1053. [PubMed: 15111519]
6. Blake GM, Fogelman I. Technical Principles of Dual Energy X-Ray Absorptiometry. Semin Nucl Med. 1997; XXVII:210–228.
7. Organization WH. Technical report. World Health Organization; Geneva: 1994. Technical report: Assessment of fracture risk and its application to screening for postmenopausal osteoporosis.
8. Kanis J. Diagnosis of osteoporosis and assessment of fracture risk. Lancet. 2002; 359:1929–36. [PubMed: 12057569]
9. Bouxsein ML. Technology Insight : noninvasive assessment of bone strength in osteoporosis. Nat Clin Pract Rheum. 2008; 4:310–318.
10. Kanis J, Johnell O, Oden A, Dawson A, De Laet C, Jonsson B. Ten year probabilities of osteoporotic fractures according to BMD and diagnostic thresholds. Osteoporosis Int. 2001; 12:989–995.

11. Schwartz AV, Sellmeyer DE. Diabetes , Fracture , and Bone Fragility. Curr Osteoporos Rep. 2007; 5:105–111. [PubMed: 17925191]
12. Siris ES, Chen YT, Abbott TA, Barrettconnor E, Miller PD, Wehren LE, Berger ML. Bone Mineral Density Thresholds for Pharmacological Intervention to Prevent Fractures. Arch Intern Med. 2004; 164:1108–12. [PubMed: 15159268]
13. Cosman F, de Beur SJ, LeBoff MS, Lewiecki EM, Tanner B, Randall S, Lindsay R. Clinicians Guide to Prevention and Treatment of Osteoporosis. Osteoporos Int. 2014
14. Nguyen N, Frost S, Center J, Eisman J, Nguyen T. Development of prognostic nomograms for individualizing 5-year and 10-year fracture risks. Osteoporos Int. 2008; 19:1431–1444. [PubMed: 18324342]
15. HippisleyCox J, Coupland C. Derivation and validation of updated QFracture algorithm to predict risk of osteoporotic fracture in primary care in the United Kingdom: prospective open cohort study. BMJ. 2012; 344:1–16.
16. Silva BC, Leslie WD, Resch H, Lamy O, Lesnyak O, Binkley N, Mccloskey EV, Kanis JA, Bilezikian JP. Trabecular Bone Score: A Noninvasive Analytical Method Based Upon the DXA Image. J Bone Miner Res. 2014; 29:518–530. [PubMed: 24443324]
17. Kanis JA, Hans D, Cooper C, Baim S, Bilezikian JP, Binkley N, Cauley Ja, Compston JE, DawsonHughes B, El-Hajj Fuleihan G, Johansson H, Leslie WD, Lewiecki EM, Luckey M, Oden A, Papapoulos SE, Poiana C, Rizzoli R, Wahl Da, McCloskey EV. Interpretation and use of FRAX in clinical practice. Osteoporosis Int. 2011; 22:2395–411.
18. Unnanuntana A, Gladnick BP, Donnelly E, Lane JM. The Assessment of Fracture Risk. J Bone Joint Surg Am. 2010; 92:743–753. [PubMed: 20194335]
19. Seeman E, Delmas PD. Bone Quality The Material and Structural Basis of Bone Strength and Fragility. N Engl J Med. 2006; 354:2250–2261. [PubMed: 16723616]
20. Boutroy S, Bouxsein ML, Munoz F, Delmas PD. In Vivo Assessment of Trabecular Bone Microarchitecture by High-Resolution Peripheral Quantitative Computed Tomography. J Clin Endocr Metab. 2005; 90:6508–6515. [PubMed: 16189253]
21. Davison KS, Kendler DL, Ammann P, Bauer DC, Dempster DW, Dian L, Hanley Da, Harris ST, McClung MR, Olszynski WP, Yuen CK. Assessing fracture risk and effects of osteoporosis drugs: bone mineral density and beyond. Am J Med. 2009; 122:992–7. [PubMed: 19854322]
22. Link TM. Osteoporosis imaging: state of the art and advanced imaging. Radiology. 2012; 263:3–17. [PubMed: 22438439]
23. Downey PA, Siegel MI. Bone Biology and the Clinical Implications for Osteoporosis. Physical Therapy. 2006; 86:77–91. [PubMed: 16386064]
24. Zioupos P, Currey JD, Hamer AJ. The role of collagen in the declining mechanical properties of aging human cortical bone. J Biomed Mater Res. 1999; 45:108–116. [PubMed: 10397964]
25. Wang X, Shen X, Li X, Agrawal CM. Age-related Changes in the Collagen Network and Toughness of Bone. Bone. 2002; 31:1–7. [PubMed: 12110404]
26. Cann CE, Genant HK. Precise Measurement of Vertebral Mineral Content Using Computed Tomography. J Comput Assist Tomo. 1980; 3:493–500.
27. Cann CE, Genant HK, Ettinger B. Quantitative Computed Tomography for Prediction of Vertebral Fracture Risk. Bone. 1985; 6:1–7. [PubMed: 3994856]
28. Beck TJ, Ruff CB, Warden KK, Scott WW, Rao GU. Predicting Femoral Neck Strength From Bone Mineral Data: A Structural Approach. Invest Radiol. 1990; 25:6–18. [PubMed: 2298552]
29. Pickhardt PJ, Pooler BD, Lauder T, Munoz del Rio A, Bruce RJ, Binkley N. Annals of Internal Medicine Opportunistic Screening for Osteoporosis Using Abdominal Computed Tomography Scans Obtained for Other Indications. Ann Intern Med. 2013; 158:588–595. [PubMed: 23588747]
30. Shepherd JA, Schousboe JT, Broy SB, Engelke K, Leslie WD. Executive Summary of the 2015 ISCD Position Development Conference on Advanced Measures From DXA and QCT : Fracture Prediction Beyond BMD. J Clin Densitom. 2016; 18:274–286.
31. Link TM, Lang TF. Axial QCT: Clinical Applications and New Developments. J Clin Densitom. 2014; 17:438–448. [PubMed: 24880494]

32. Cheng X, Li J, Lu Y, Keyak J, Lang T. Proximal femoral density and geometry measurements by quantitative computed tomography : Association with hip fracture. Bone. 2007; 40:169–174. [PubMed: 16876496]
33. Black DM, Bouxsein ML, Marshall LM, Cummings SR, Lang TF, Cauley JA. Proximal Femoral Structure and the Prediction of Hip Fracture in Men: A Large Prospective Study Using QCT. J Bone Miner Res. 2008; 23:1326–1333. [PubMed: 18348697]
34. RodriguezSoto AE, Fritscher KD, Schuler B, Issever AS, Roth T, Kamelger F, Kammerlander C, Blauth M, Schubert R, Link TM. Texture Analysis, Bone Mineral Density, and Cortical Thickness of the Proximal Femur: Fracture Risk Prediction. J Comput Assist Tomo. 2010; 34:949–957.
35. Yu W, Glfier CC, Grampp S, Jergas M, Fuerst T, Wu CY, Lu Y, Fan B, Genant HK. Spinal Bone Mineral Assessment in Postmenopausal Women : A Comparison Between Dual X-ray Absorptiometry and Quantitative Computed Tomography. Osteoporos Int. 1995; 5:433–439. [PubMed: 8695964]
36. Bergot C, LavalJeantet A, Hutchinson K, Dautraix I, Caulin F, Genant H. A comparison of spinal quantitative computed tomography with dual energy x-ray absorptiometry in European women with vertebral and nonvertebral fractures. Calcif Tissue Int. 2001; 68:74–82. [PubMed: 11310350]
37. Ito M, Ikeda K, Nishiguchi M, Shindo H, Uetani M, Hosoi T, Orimo H. Multi-Detector Row CT Imaging of Vertebral Microstructure for Evaluation of Fracture Risk. J Bone Miner Res. 2005; 20:1828–1836. [PubMed: 16160740]
38. Manske SL, LiuAmbrose T, Bakker PM, Liu D, Kontulainen S, Guy P, Oxland T, McKay H. Femoral neck cortical geometry measured with magnetic resonance imaging is associated with proximal femur strength. Osteoporosis Int. 2006; 17:1539–1545.
39. Zysset PK, Ara ED, Varga P, Pahr DH. Finite element analysis for prediction of bone strength. BoneKEy Reports. 2013; 386:1–9.
40. Imai K. Computed tomography-based finite element analysis to assess fracture risk and osteoporosis treatment. World J Exp Med. 2015; 5:182–188. [PubMed: 26309819]
41. Hernandez CJ, Cresswell EN. Understanding Bone Strength from Finite Element Models: Concepts for Non-engineers. Clinic Rev Bone Miner Metab. 2016; 14:161–166.
42. Keyak JH, Rossi Sa, Jones Ka, Skinner HB. Prediction of femoral fracture load using automated finite element modeling. J Biomech. 1998; 31:125–33. [PubMed: 9593205]
43. Crawford R, Cann CE, Keaveny TM. Finite element models predict in vitro vertebral body compressive strength better than quantitative computed tomography. Bone. 2003; 33:744–750. [PubMed: 14555280]
44. Orwoll ES, Marshall LM, Nielson CM, Cummings SR, Lapidus J, Cauley JA, Ensrud K, Lane N, Hoffmann PR, Kopperdahl DL, Keaveny TM. Finite Element Analysis of the Proximal Femur and Hip Fracture Risk in Older Men. J Bone Miner Res. 2009; 24:475–83. [PubMed: 19049327]
45. Keyak JH, Sigurdsson S, Karlsdottir G, Oskarsdottir D, Sigmarsdottir A, Zhao S, Kornak J, Harris TB, Sigurdsson G, Jonsson BY, Siggeirsdottir K, Eiriksdottir G, Gudnason V, Lang TF. Male female differences in the association between incident hip fracture and proximal femoral strength: A finite element analysis study. Bone. 2011; 48:1239–1245. [PubMed: 21419886]
46. Kopperdahl DL, Aspelund T, Hoffmann PF, Sigurdsson S, Siggeirsdottir K, Harris TB, Gudnason V, Keaveny TM. Assessment of Incident Spine and Hip Fractures in Women and Men Using Finite Element Analysis of CT Scans. J Bone Miner Res. 2014; 29:570–580. [PubMed: 23956027]
47. Laib A, Häuselmann JH, Rüegsegger P. In vivo high resolution 3D-QCT of the human forearm. Technology and health care: official journal of the European Society for Engineering and Medicine. 1998; 6:329–337. [PubMed: 10100936]
48. Kabel J, Odgaard A, van Rietbergen B, Huiskes R. Connectivity and the Elastic Properties of Cancellous Bone. Bone. 1999; 24:115–120. [PubMed: 9951779]
49. Odgaard A. Three-Dimensional Methods for Quantification of Cancellous Bone Architecture. Bone. 1997; 20:315–328. [PubMed: 9108351]
50. Hildebrand TOR, Rüegsegger P. Quantification of Bone Microarchitecture with the Structure Model Index. Comput Method Biomec Biomed Eng. 1997; 1:15–23.
51. Liu XS, Sajda P, Saha PK, Wehrli FW, Bevill G, Keaveny TM, Guo XE. Complete Volumetric Decomposition of Individual Trabecular Plates and Rods and Its Morphological Correlations With

Anisotropic Elastic Moduli in Human Trabecular Bone. J Bone Miner Res. 2008; 23:223–235. [PubMed: 17907921]

52. Burrows M, Liu D, McKay H. High-resolution peripheral QCT imaging of bone microstructure in adolescents. Osteoporosis Int. 2010; 21:515–20.
53. Nishiyama KK, Pauchard Y, Nikkel LE, Iyer S, Zhang C, Mcmahon DJ, Cohen D, Boyd SK, Shane E, Nickolas TL. Longitudinal HR pQCT and Image Registration Detects Endocortical Bone Loss in Kidney Transplantation Patients. J Bone Miner Res. 2015; 30:554–561. [PubMed: 25213758]
54. SornayRendu E, Boutroy S, Munoz F, Delmas PD. Alterations of Cortical and Trabecular Architecture Are Associated With Fractures in Postmenopausal Women, Partially Independent of Decreased BMD Measured by DXA: The OFELY Study. J Bone Miner Res. 2007; 22:425–433. [PubMed: 17181395]
55. Liu XS, Stein EM, Zhou B, Zhang Ca, Nickolas TL, Cohen A, Thomas V, McMahon DJ, Cosman F, Nieves J, Shane E, Guo XE. Individual trabecula segmentation (ITS)- based morphological analyses and microfinite element analysis of HR-pQCT images discriminate postmenopausal fragility fractures independent of DXA measurements. J Bone Miner Res. 2012; 27:263–72. [PubMed: 22072446]
56. Macdonald HM, Nishiyama KK, Kang J, Hanley DA, Boyd SK. Age-Related Patterns of Trabecular and Cortical Bone Loss Differ Between Sexes and Skeletal Sites: A Population-Based HR-pQCT Study. J Bone Miner Res. 2011; 26:50–62. [PubMed: 20593413]
57. Paccou J, Ward KA, Jameson KA, Dennison EM, Cooper C, Edwards MH. Bone Microarchitecture in Men and Women with Diabetes: The Importance of Cortical Porosity. Calcif Tissue Int. 2016; 98:465–473. [PubMed: 26686695]
58. Kazakia GJ, Tjong W, Nirody Ja, Burghardt AJ, CarballidoGamio J, Patsch JM, Link T, Feeley BT, Ma CB. The influence of disuse on bone microstructure and mechanics assessed by HR-pQCT. Bone. 2014; 63:132–40. [PubMed: 24603002]
59. Pistoia W, van Rietbergen B, Lochmüller EM, Lill Ca, Eckstein F, Rüegsegger P. Estimation of distal radius failure load with micro-finite element analysis models based on three-dimensional peripheral quantitative computed tomography images. Bone. 2002; 30:842–8. [PubMed: 12052451]
60. Khosla S, Riggs BL, Atkinson EJ, Oberg AL, McDaniel LJ, Holets M, Peterson JM, Melton LJ. Effects of sex and age on bone microstructure at the ultradistal radius: a population-based noninvasive in vivo assessment. J Bone Miner Res. 2006; 21:124–31. [PubMed: 16355281]
61. Melton LJ, Riggs BL, Lenthe GHV, Achenbach SJ, Müller R, Bouxsein ML, Amin S, Atkinson EJ, Khosla S. Contribution of In Vivo Structural Measurements and Load- /Strength Ratios to the Determination of Forearm Fracture Risk in Postmenopausal Women. J Bone Miner Res. 2007; 22:1442–1448. [PubMed: 17539738]
62. Vico L, Zouch M, Amirouche A, Frère D, Laroche N, Koller B, Laib A, Thomas T, Alexandre C. High-Resolution pQCT Analysis at the Distal Radius and Tibia Discriminates Patients With Recent Wrist and Femoral Neck Fractures. J Bone Miner Res. 2008; 23:1741–1750. [PubMed: 18665795]
63. Boutry S, Brunin S, Mahieu I, Laurent S, Vander Elst L, Muller RN. Magnetic labeling of non-phagocytic adherent cells with iron oxide nanoparticles: a comprehensive study. Contrast Media Mol I. 2008; 3:223–32.
64. Stein EM, Liu XS, Nickolas TL, Cohen A, Thomas V, Mcmahon DJ, Zhang C, Yin PT, Cosman F, Nieves J, Guo XE, Shane E. J BMR Abnormal Microarchitecture and Reduced Stiffness at the Radius and Tibia in Postmenopausal Women With Fractures. J Bone Miner Res. 2010; 25:2572–2581. [PubMed: 20564238]
65. SornayRendu E, CabreraBravo JL, Boutroy S, Munoz F, Delmas PD. Severity of Vertebral Fractures Is Associated With Alterations of Cortical Architecture in Postmenopausal Women. J Bone Miner Res. 2009; 24:737–743. [PubMed: 19113929]
66. Stein EM, Liu XS, Nickolas TL, Cohen A, Mcmahon DJ, Zhou B, Zhang C, KamandaKosseh M, Cosman F, Nieves J, Guo XE, Shane E. Microarchitectural Abnormalities Are More Severe in Postmenopausal Women with Vertebral Compared to Nonvertebral Fractures. J Clin Endocr Metab. 2012; 97:1918–1926.

67. Mueller TL, Wirth AJ, Lenthe GHV, Goldhahn J, Schense J, Jamieson V, Messmer P, Uebelhart D, Weishaupt D, Egermann M, Muller R. Mechanical stability in a human radius fracture treated with a novel tissue-engineered bone substitute : a non-invasive , longitudinal assessment using high-resolution pQCT in combination with finite element analysis. J Tissue Eng Regen M. 2011; 5:415–420. [PubMed: 20827669]
68. De Jong JJ, Willems PC, Arts JJ, Bours SGP, Brink PRG, van Geel TA, Poeze M, Geusens PP, van Rietbergen B, van den Bergh JPW. Assessment of the healing process in distal radius fractures by high resolution peripheral quantitative computed tomography. Bone. 2014; 64:65–74. [PubMed: 24704263]
69. Christen D, Melton LJ, Zwahlen A, Amin S, Khosla S, Müller R. Improved Fracture Risk Assessment Based on Nonlinear Micro Finite Element Simulations From HRpQCT Images at the Distal Radius. J Bone Miner Res. 2013; 28:2601–2608. [PubMed: 23703921]
70. Damilakis J, Adams JE, Guglielmi G, Link TM. Radiation exposure in X-ray-based imaging techniques used in osteoporosis. Eur Radiol. 2010; 20:2707–2714. [PubMed: 20559834]
71. Gregg E, Kriska A, Salamone L, Roberts M, Anderson S, Ferrell R, Kuller L, Cauley J. The Epidemiology of Quantitative Ultrasound: A Review of the Relationships with Bone Mass, Osteoporosis and Fracture Risk. Osteoporosis Int. 1997; 7:89–99.
72. Guglielmi G, Terlizzi FD. Quantitative Ultrasond in the assessment of Osteoporosis. Eur J Radiol. 2009; 71:425–431. [PubMed: 19651483]
73. Bouxsein ML, Coan BS, Lee SC. Prediction of the strength of the elderly proximal femur by bone mineral density and quantitative ultrasound measurements of the heel and tibia. Bone. 1999; 25:49–54. [PubMed: 10423021]
74. Trimpou P, Bosaeus I, Bengtsson BA, LandinWiilhelmsen K. High correlation between quantitative ultrasound and DXA during 7 years of follow-up. Eur J Radiol. 2010; 73:360–364. [PubMed: 19135327]
75. Moayyeri A, Adams JE, Adler RA, Krieg M, Hans D, Compston J, Lewiecki EM. Quantitative ultrasound of the heel and fracture risk assessment : an updated metaanalysis. Osteoporos Int. 2012; 23:143–153. [PubMed: 22037972]
76. Chan MY, Nguyen ND, Center JR, Eisman JA, Nguyen TV. Absolute Fracture-Risk Prediction by a Combination of Calcaneal Quantitative Ultrasound and Bone Mineral Density. Calcif Tissue Int. 2012; 90:128–136. [PubMed: 22179560]
77. Chan MY, Nguyen ND, Center JR, Eisman JA, Nguyen TV. Quantitative ultrasound and fracture risk prediction in non-osteoporotic men and women as defined by WHO criteria. Osteoporos Int. 2013; 24:1015–1022. [PubMed: 22878531]
78. Kauppi M, Impivaara O, Mäki J, Heliövaara M, Jula A. Quantitative ultrasound measurements and vitamin D status in the assessment of hip fracture risk in a nationally representative population sample. Osteoporos Int. 2013; 24:2611–2618. [PubMed: 23595563]
79. Damilakis J, Papadokostakis G, Perisinakis K, Maris TG, Karantanas AH. Hip fracture discrimination by the Achilles Insight QUS imaging device. Eur J Radiol. 2007; 63:59–62. [PubMed: 17478068]
80. Hans D, Krieg Ma. The Clinical Use of Quantitative Ultrasound (QUS) in the Detection and Management of Osteoporosis. IEEE T Ultrason Ferr. 2008:55.
81. Zhang L, Lv H, Zheng H, Li M, Yin P, Peng Y, Gao Y, Zhang L, Tang P. Correlation between Parameters of Calcaneal Quantitative Ultrasound and Hip Structural Analysis in Osteoporotic Fracture Patients. PloS one. 2015:1–14.
82. McLeod KM, Johnson S, Rasali D, Verma A. Discriminatory Performance of the Calcaneal Quantitative Ultrasound and Osteoporosis Self-Assessment Tool to Select Older Women for Dual-Energy X-ray Absorptiometry. J Clin Densitom. 2016; 18:157–164.
83. Villa P, Lassandro A, Moruzzi M, Amar I, Vacca L, Di Nardo F, De Waure C, Pontecorvi A, Scambia G. A non invasive prevention program model for the assessment of osteoporosis in the early postmenopausal period : a pilot study on FRAX and QUS tools advantages. J Endocrinol Invest. 2016; 39:191–198. [PubMed: 26141076]
84. Briot K. What is the role of DXA , QUS and bone markers in fracture prediction, treatment allocation and monitoring ? Best Pract Res Cl Rh. 2005; 19:951–964.

85. Guglielmi G, Adams J, Link TM. Quantitative ultrasound in the assessment of skeletal status. Eur Radiol. 2009; 19:1837–48. [PubMed: 19259681]

86. Majumdar S, Genant HK, Grampp S, Newitt DC, Truong VH, Lin JC, Mathur A. Correlation of trabecular bone structure with age, bone mineral density, and osteoporotic status: in vivo studies in the distal radius using high resolution magnetic resonance imaging. J Bone Miner Res. 1997; 12:111–8. [PubMed: 9240733]

87. Majumdar S. Magnetic Resonance Imaging of Trabecular Bone Structure. Topics in Magn Reson Img. 2002; 13:323–334.

88. Wehrli, FW., Song, HK., Saha, PK., Wright, AC. Quantitative MRI for the assessment of bone structure and function y. 2006. p. 731-764.

89. Wehrli FW. Structural and Functional Assessment of Trabecular and Cortical Bone by Micro Magnetic Resonance Imaging. J Magn Reson Img. 2007; 409:390–409.

90. Krug R, CarballidoGamio J, Burghardt AJ, Kazakia G, Hyun BH, Jobke B, Banerjee S, Huber M, Link TM, Majumdar S. Assessment of trabecular bone structure comparing magnetic resonance imaging at 3 Tesla with high-resolution peripheral quantitative computed tomography ex vivo and in vivo. Osteoporos Int. 2008; 19:653–661. [PubMed: 17992467]

91. Boutry N, Cortet B, Dubois P, Marchandise X, Cotten A. Radiology Trabecular Bone Structure of the Calcaneus: Preliminary in Vivo MR Imaging Assessment in Men with Osteoporosis. Radiology. 2003; 227:708–717. [PubMed: 12676974]

92. Chesnut CH, Majumdar S, Newitt DC, Shields A, Pelt JV, Laschansky E, Azria M, Kriegman A, Olson M, Eriksen EF, Mindeholm L. Effects of Salmon Calcitonin on Trabecular Microarchitecture as Determined by Magnetic Resonance Imaging : Results From the QUEST Study. J Bone Miner Res. 2005; 20:1548–1561. [PubMed: 16059627]

93. Banerjee S, Han ET, Krug R, Newitt DC, Majumdar S. Application of Refocused Steady-State Free- Precession Methods at 1. 5 and 3 T to In Vivo High- Resolution MRI of Trabecular Bone : Simulations and Experiments. J Magn Reson Img. 2005; 21:818–825.

94. Techawiboonwong A, Song HK, Magland JF, Saha PK, Wehrli FW. Implications of Pulse Sequence in Structural Imaging of Trabecular Bone. J Magn Reson Img. 2005; 22:647–655.

95. Ma J, Wehrli FW, Song HK. Fast 3D Large-Angle Spin-Echo Imaging (3D FLASE). Magn Reson Med. 1996; 35:903–910. [PubMed: 8744019]

96. Song HK, Wehrli FW. In Vivo Micro-Imaging Using Alternating Navigator Echoes With Applications to Cancellous Bone Structural Analysis. Magn Reson Med. 1999; 953:947–953.

97. Vasilic B, Wehrli FW. A Novel Local Thresholding Algorithm for Trabecular Bone Volume Fraction Mapping in the Limited Spatial Resolution Regime of In Vivo MRI. IEEE T Med Imaging. 2005; 24:1574–1585.

98. Krug R, Banerjee S, Han ET, Newitt DC, Link TM, Majumdar S. Feasibility of in vivo structural analysis of high-resolution magnetic resonance images of the proximal femur. Osteoporosis Int. 2005; 16:1307–14.

99. Chang G, Deniz CM, Honig S, Egol K, Regatte RR, Zhu Y, Sodickson DK, Brown R. MRI of the Hip at 7T : Feasibility of Bone Microarchitecture , High-Resolution Cartilage , and Clinical Imaging. J Magn Reson Img. 2014; 39:1384–1393.

100. Hotca A, Rajapakse CS, Cheng C, Honig S, Egol K, Regatte RR, Saha PK, Chang G. In Vivo Measurement Reproducibility of Femoral Neck Microarchitectural Parameters Derived From 3T MR Images. J Magn Reson Img. 2015; 42:1339–1345.

101. Wehrli FW, Gomberg BR, Saha PK, Song HEEK, Hwang SN, Snyder PJ. Digital Topological Analysis of In Vivo Magnetic Resonance Microimages of Trabecular Bone Reveals Structural Implications of Osteoporosis. J Bone Miner Res. 2001; 16:1520–1531. [PubMed: 11499875]

102. Laib A, Newitt DC, Lu Y, Majumdar S. New Model-Independent Measures of Trabecular Bone Structure Applied to In Vivo High-Resolution MR Images. Osteoporos Int. 2002; 13:130–136. [PubMed: 11905523]

103. VanRietbergen B, Majumdar S, Newitt D, MacDonald B. High-resolution MRI and micro-FE for the evaluation of changes in bone mechanical properties during longitudinal clinical trials: application to calcaneal bone in postmenopausal women after one year of idoxifene treatment. Clin Biomech. 2002; 17:81–88.

104. Zhang XH, Liu XS, Vasilic B, Wehrli FW, Benito M, Rajapakse CS, Snyder PJ, Guo XE. In Vivo micro-MRI-Based Finite Element and Morphological Analyses of Tibial Trabecular Bone in Eugonadal and Hypogonadal Men Before and After Testosterone Treatment. J Bone Miner Res. 2008; 23:1426–1434. [PubMed: 18410234]

105. Wehrli FW, Rajapakse CS, Magland JF, Snyder PJ. Mechanical Implications of Estrogen Supplementation in Early Postmenopausal Women. J Bone Miner Res. 2010; 25:1406–1414. [PubMed: 20200948]

106. Sharma GB, Robertson DD, Laney DA, Gambello MJ, Terk M. Machine learning based analytics of micro-MRI trabecular bone microarchitecture and texture in type 1 Gaucher disease. J Biomech. 2016; 49:1961–1968. [PubMed: 27109052]

107. Chang G, Rajapakse CS, Babb JS, Honig SP, Recht MP, Regatte RR. In vivo estimation of bone stiffness at the distal femur and proximal tibia using ultra-high-field 7-Tesla magnetic resonance imaging and micro-finite element analysis. Journal of bone and mineral metabolism. 2012; 30:243–51. [PubMed: 22124539]

108. Zhang N, Magland JF, Rajapakse CS, Bhagat YA, Wehrli FW. Potential of in vivo MRIbased nonlinear finite-element analysis for the assessment of trabecular bone post-yield properties. Med Phys. 2013; 40:1–10.

109. Rajapakse CS, Leonard MB, Bhagat YA, Sun W, Magland JF, Wehrli FW. Micro-MR Imaging-based Computational Biomechanics Demonstrates Reduction in Cortical and Trabecular Bone Strength after Renal Transplantation. Radiology. 2012:262. [PubMed: 22025733]

110. Chang G, Deniz CM, Honig S, Rajapakse CS, Egol K, Regatte RR, Brown R. Feasibility of three dimensional MRI of proximal femur microarchitecture at 3 tesla using 26 receive elements without and with parallel imaging. J Magn Reson Img. 2014; 40:229–38.

111. Chang G, Rajapakse CS, Regatte RR, Babb J, Saxena A, Belmont HM, Honig S. 3 Tesla MRI Detects Deterioration in Proximal Femur Microarchitecture and Strength in Long-term Glucocorticoid Users Compared With Controls. J Magn Reson Img. 2015; 42:1489–1496.

112. Folkesson J, Goldenstein J, Carballidogamio J, Kazakia G, Burghardt AJ, Rodriguez A, Krug R, Papp AED, Link TM, Majumdar S. Longitudinal evaluation of the effects of alendronate on MRI bone microarchitecture in postmenopausal osteopenic women. Bone. 2011; 48:611–621. [PubMed: 21059422]

113. Gomberg BR, Wehrli FW, Vasilic B, Weening RH, Saha PK, Song HK, Wright AC. Reproducibility and error sources of micro-MRI-based trabecular bone structural parameters of the distal radius and tibia. Bone. 2004; 35:266–276. [PubMed: 15207767]

114. Vasilic B, Ladinsky GA, Saha PK, Wehrli FW. Micro-MRI-Based Image Acquisition and Processing System for Assessing the Response to Therapeutic Intervention. Proc of SPIE. 2006; 6143:1–11.

115. Justesen J, Stenderup K, Ebbesen EN, Mosekilde L, Steiniche T, Kassem M. Adipocyte tissue volume in bone marrow is increased with aging and in patients with osteoporosis. Biogerontology. 2001; 2:165–171. [PubMed: 11708718]

116. Rosen CJ, Bouxsein ML. Mechanisms of Disease: is osteoporosis the obesity of bone ? Nat Clin Pract Rheum. 2006; 2:35–43.

117. Fazeli PK, Horowitz MC, Macdougald OA, Scheller EL, Rodeheffer MS, Rosen CJ, Klibanski A. Marrow Fat and Bone New Perspectives. J Clin Endocr Metab. 2013; 98:935–945. [PubMed: 23393168]

118. Yeung DKW, Griffith JF, Antonio GE, Lee FKH, Woo J, Leung PC. Osteoporosis is associated with increased marrow fat content and decreased marrow fat unsaturation: a proton MR spectroscopy study. J Magn Reson Img. 2005; 22:279–85.

119. Schellinger D, Lin CS, Hatipoglu HG, Fertikh D. Potential Value of Vertebral Proton MR Spectroscopy in Determining Bone Weakness. Am J Neuroradiol. 2001; 22:1620–1627. [PubMed: 11559519]

120. Wehrli FW, Hopkins Ja, Hwang SN, Song HK, Snyder PJ, Haddad JG. Cross-sectional study of osteopenia with quantitative MR imaging and bone densitometry. Radiology. 2000; 217:527–38. [PubMed: 11058656]

121. Machann J, Stefan N, Schick F. H MR spectroscopy of skeletal muscle , liver and bone marrow. Eur J Radiol. 2008; 67:275–284. [PubMed: 18406092]

122. Ren J, Dimitrov I, Sherry AD, Malloy CR. Composition of adipose tissue and marrow fat in humans by 1 H NMR at 7 Tesla. J Lipid Res. 2008; 49:2055–2062. [PubMed: 18509197]

123. Li X, Kuo D, Schafer AL, Porzig A, Link TM, Black D, Schwartz AV. Quantification of vertebral bone marrow fat content using 3 Tesla MR spectroscopy: reproducibility, vertebral variation, and applications in osteoporosis. J Magn Reson Img. 2011; 33:974–9.

124. Verma S, Rajaratnam JH, Denton J, Hoyland JA, Byers RJ. Adipocytic proportion of bone marrow is inversely related to bone formation in osteoporosis. J Clin Pathol. 2002; 55:693–698. [PubMed: 12195001]

125. Patsch JM, Li X. Bone marrow composition, diabetes, and fracture risk: more bad news for saturated fat. J Bone Miner Res. 2013; 28:1718–20. [PubMed: 23794182]

126. Krings A, Rahman S, Huang S, Lu Y, Czernik PJ, LeckaCzernik B. Bone marrow fat has brown adipose tissue characteristics , which are attenuated with aging and diabetes. Bone. 2012; 50:546–552. [PubMed: 21723971]

127. Baum T, Yap SP, Karampinos DC, Nardo L, Kuo D, Burghardt AJ, Masharani UB, Schwartz AV, Li X, Link TM. Does Vertebral Bone Marrow Fat Content Correlate With Abdominal Adipose Tissue , Lumbar Spine Bone Mineral Density , and Blood Biomarkers in Women With Type 2 Diabetes Mellitus ? J Magn Reson Img. 2012; 35:117–124.

128. Ni Q, Nyman JS, Wang X, Santos ADL, Nicolella DP. Assessment of water distribution changes in human cortical bone by nuclear magnetic resonance. Measurement Science and Technology. 2007; 18:715–723.

129. Horch RA, Nyman JS, Gochberg DF, Dortch RD, Does MD. Characterization of 1H NMR signal in human cortical bone for magnetic resonance imaging. Magn Reson Med. 2010; 64:680–7. [PubMed: 20806375]

130. Ong HH, Wright AC, Wehrli FW. Deuterium nuclear magnetic resonance unambiguously quantifies pore and collagen-bound water in cortical bone. J Bone Miner Res. 2012; 27:2573–2581. [PubMed: 22807107]

131. Fantazzini P, Brown RJS, Borgia GC. Bone tissue and porous media: common features and differences studied by NMR relaxation. Magn Reson Img. 2003; 21:227–234.

132. Robson MD, Gatehouse PD, Bydder M, Bydder GM. Magnetic Resonance : An introduction to Ultrashort TE (UTE) imaging. J Comput Assist Tomo. 2003; 27:825– 846.

133. Wu Y, Ackerman JL, Chesler Da, Graham L, Wang Y, Glimcher MJ. Density of organic matrix of native mineralized bone measured by water- and fat-suppressed proton projection MRI. Magnetic resonance in medicine : official journal of the Society of Magnetic Resonance in Medicine / Society of Magnetic Resonance in Medicine. 2003; 50:59–68.

134. Weiger M, Pruessmann KP, Hennel F. MRI with zero echo time: hard versus sweep pulse excitation. Magn Reson Med. 2011; 66:379–89. [PubMed: 21381099]

135. Idiyatullin D, Corum C, Park JY, Garwood M. Fast and quiet MRI using a swept radiofrequency. J Magn Reson. 2006; 181:342–9. [PubMed: 16782371]

136. Robson MD, Gatehouse PD, Bydder M, Bydder GM. Magnetic Resonance: An introduction to Ultrashort TE (UTE) imaging. J Comput Assist Tomo. 2003; 27:825–846.

137. Diaz E, Chung CB, Bae WC, Statum S, Znamirowski R, Bydder GM, Du J. Ultrashort echo time spectroscopic imaging (UTESI): an efficient method for quantifying bound and free water. NMR Biomed. 2012; 25:161–8. [PubMed: 21766381]

138. Techawiboonwong A, Song HK, Wehrli FW. In vivo MRI of submillisecond T 2 species with two-dimensional and three-dimensional radial sequences and applications to the measurement of cortical bone water. NMR Biomed. 2008; 21:59–70. [PubMed: 17506113]

139. Techawiboonwong A, Song HK, Leonard MB, Wehrli FW. Cortical Bone Water: in vivo quantification with ultrashort echo-time MR imaging. Radiology. 2008; 248:824–833. [PubMed: 18632530]

140. Du J, Carl M, Bydder M, Takahashi A, Chung CB, Bydder GM. Qualitative and quantitative ultrashort echo time (UTE) imaging of cortical bone. J Magn Reson. 2010; 207:304–11. [PubMed: 20980179]

141. Bae WC, Chen PC, Chung CB, Masuda K, D'Lima D, Du J. Quantitative ultrashort echo time (UTE) MRI of human cortical bone: correlation with porosity and biomechanical properties. J Bone Miner Res. 2012; 27:848–57. [PubMed: 22190232]

142. Rad HS, Lam SCB, Magland JF, Ong H, Li C, Song HK, Love J, Wehrli FW. Quantifying cortical bone water in vivo by three-dimensional ultra-short echo-time MRI. NMR Biomed. 2011; 24:855–64. [PubMed: 21274960]

143. Manhard MK, Horch RA, Gochberg DF, Nyman JS, Does MD. In Vivo Quantitative MR Imaging of Bound and Pore Water in Cortical Bone. Radiology. 2015; 277:221–229. [PubMed: 26020434]

144. Rajapakse CS, BashoorZadeh M, Li C, Sun W, Wright AC, Wehrli FW. Volumetric Cortical Bone Porosity Assessment with MR Imaging : Validation and Clinical Feasibility. Radiology. 2015; 276:526–535. [PubMed: 26203710]

145. Nyman JS, Ni Q, Nicolella DP, Wang X. Measurements of mobile and bound water by nuclear magnetic resonance correlate with mechanical properties of bone. Bone. 2008; 42:193–9. [PubMed: 17964874]

146. Horch RA, Gochberg DF, Nyman JS, Does MD. Non-invasive predictors of human cortical bone mechanical properties: T(2)-discriminated H NMR compared with high resolution X-ray. PloS one. 2011; 6:e16359. [PubMed: 21283693]

147. Seifert AC, Wehrli FW. Solid-State Quantitative 1 H and 31 P MRI of Cortical Bone in Humans. Curr Osteoporos Rep. 2016; 14:77–86. [PubMed: 27048472]

148. Du J, Diaz E, Carl M, Bae W, Chung CB, Bydder GM. Ultrashort echo time imaging with bicomponent analysis. Magn Reson Med. 2012; 67:645–9. [PubMed: 22034242]

149. Du J, Hermida JC, Diaz E, Corbeil J, Znamirowski R, D'Lima DD, Bydder GM. Assessment of cortical bone with clinical and ultrashort echo time sequences. Magn Reson Med. 2013; 70:697–704. [PubMed: 23001864]

150. Li C, Seifert AC, Rad HS, Bhagat YA, Rajapakse CS, Sun W, Lam SCB, Wehrli FW. Cortical Bone Water Concentration : Dependence of MR Imaging Measures on Age and Pore Volume Fraction. Radiology. 2014; 272:796–806. [PubMed: 24814179]

151. Ni Q, King JD, Wang X. The characterization of human compact bone structure changes by low-field nuclear magnetic resonance. Meas Sci Technol. 2004; 15:58–66.

152. Horch RA, Gochberg DF, Nyman JS, Does MD. Clinically compatible MRI strategies for discriminating bound and pore water in cortical bone. Magn Reson Med. 2012; 68:1774–84. [PubMed: 22294340]

153. Li C, Seifert A, Magland J, Wehrli F. Zero Echo Time (ZTE) imaging with anisotropic field-of-view. Proc Intl Soc Magn Reson Med. 2013; 21:762.

154. Seifert AC, Wehrli SL, Wehrli FW. Bi-component T2 * analysis of bound and pore bone water fractions fails at high field strengths. NMR in biomedicine. 2015; 28:861–72. [PubMed: 25981785]

155. Manhard MK, Horch RA, Harkins KD, Gochberg DF, Nyman JS, Does MD. Validation of quantitative bound- and pore-water imaging in cortical bone. Magn Reson Med. 2014; 71:2166–2171. [PubMed: 23878027]

156. Manhard MK, Uppuganti S, Granke M, Gochberg DF, Nyman JS, Does MD. MRIderived bound and pore water concentrations as predictors of fracture resistance. Bone. 2016; 87:1–10. [PubMed: 26993059]

157. Larson PEZ, Conolly SM, Pauly JM, Nishimura DG. Using adiabatic inversion pulses for long-T2 suppression in ultrashort echo time (UTE) imaging. Magn Reson Med. 2007; 58:952–61. [PubMed: 17969119]

158. Li C, Magland JF, Rad HS, Song HK, Wehrli FW. Comparison of optimized soft-tissue suppression schemes for ultrashort echo time MRI. Magnetic resonance in medicine : official journal of the Society of Magnetic Resonance in Medicine / Society of Magnetic Resonance in Medicine. 2011; 689:680–689.

159. Seifert AC, Li C, Rajapakse CS, Bashoorzadeh M, Bhagat YA, Wright AC, Zemel BS, Zavaliangos A, Wehrli FW. Bone mineral 31 P and matrix-bound water densities measured by solid-state 31 P and 1 H MRI. NMR Biomed. 2014; 27:739–748. [PubMed: 24846186]

160. Gatehouse P, Bydder G. Magnetic Resonance Imaging of Short T2 Components in Tissue. Clinical Radiology. 2003; 58:1–19. [PubMed: 12565203]

161. Atkinson IC, Lu A, Thulborn KR. Characterization and correction of system delays and eddy currents for MR imaging with ultrashort echo-time and time-varying gradients. Magn Reson Med. 2009; 62:532–7. [PubMed: 19353662]

162. Harkins KD, Does MD, Grissom WA. Iterative method for predistortion of MRI gradient waveforms. IEEE T Med Imaging. 2014; 33:1641–1647.

163. Manhard MK, Harkins KD, Gochberg DF, Nyman JS, Does MD. 30-Second Boundand Pore-Water Maps of Cortical Bone. Int Soc Magn Res Med, In: Int Soc Magn Res Med. 2016:676.

164. Geusens P, Chapurlat R, Schett G, Ghasemzadeh A, Seeman E, Jong JD, van den Bergh J. High-resolution in vivo imaging of bone and joints : a window to microarchitecture. Nat Rev Rheumatol. 2014; 10:304–313. [PubMed: 24595090]

165. Chang G, Honig S, Brown R, Deniz CM, Egol K, Babb JS, Regatte RR, Rajapakse CS. Finite Element Analysis Applied to 3-T MR Imaging of Proximal Femur Microarchitecture: Lower Bone Strength in Patients with Fragility Fractures Compared with Control Subjects. Radiolgoy. 2014; 272:464–474.

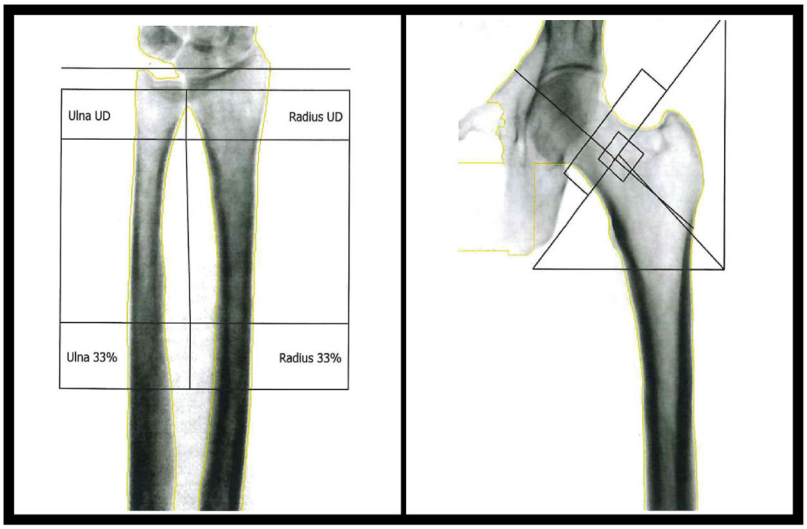

Figure 1.
Representative DXA scans acquired in the forearm (left) and the hip (right).

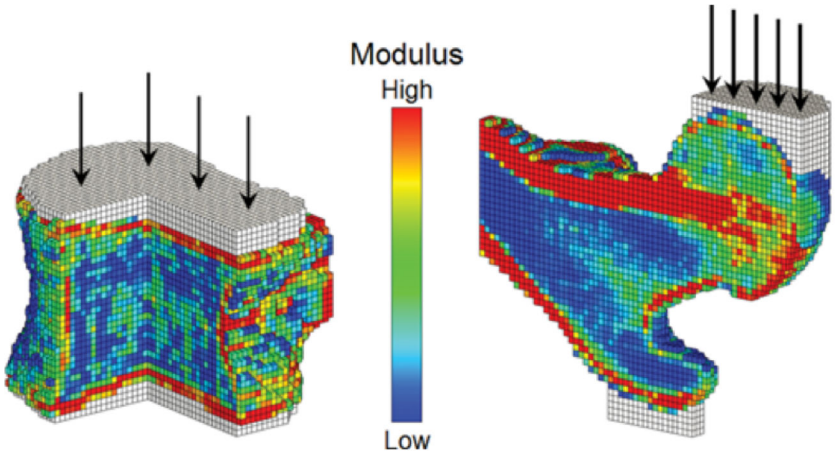

Figure 2.

Assessment of incident spine and hip fractures in women and men using finite element analysis of CT scans: Sectioned views of finite element models of a vertebral body (left) and a proximal femur (right) showing the distribution of elastic modulus. Applied loads, which simulate axial compression for the spine and an unprotected sideways fall for the hip, are shown schematically, applied through layers of bone cement (white elements) to distribute the load over the bone surface. Reproduced from (46).

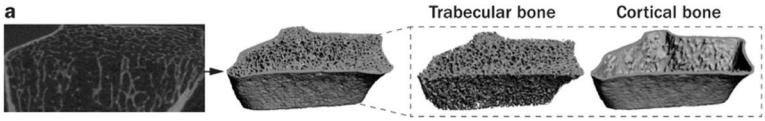

Figure 3.

Segmentation of forearm cortical and trabecular bone in HR-pQCT images. Reproduced in part from (164).

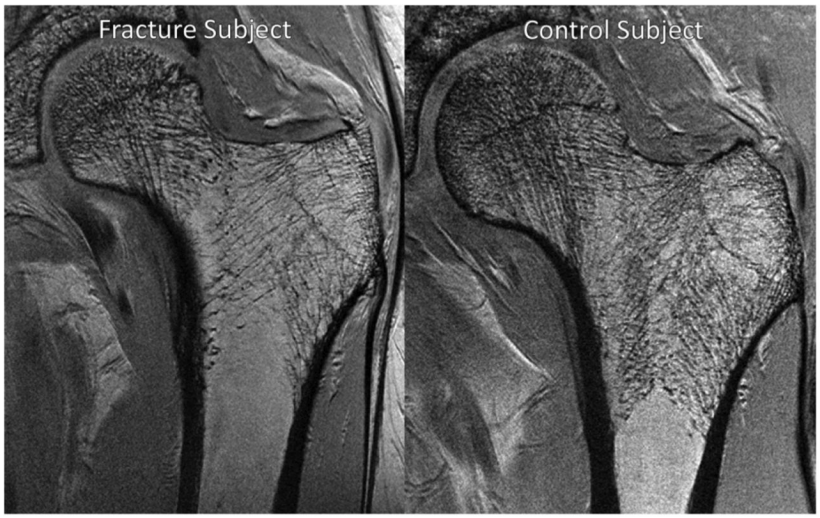

Figure 4.

Representative coronal high-spatial-resolution 3-T MR images of proximal femur microarchitecture in a subject with osteoporotic fracture (left panel) and a control subject (right panel). Trabeculae are hypointense linear foci. There is deterioration in trabecular microarchitecture in the fracture subject compared with the control subject. Reproduced from (165).

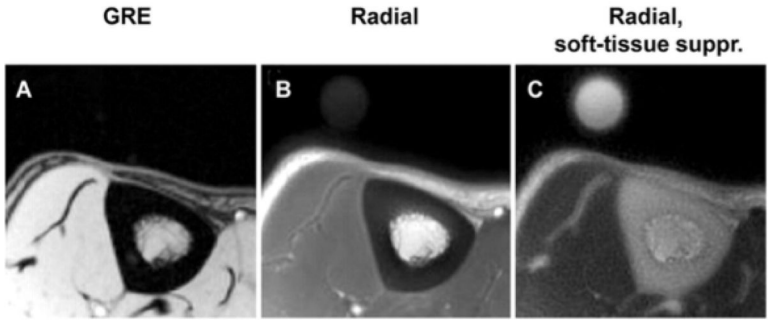

Figure 5.

Representative transverse MR images of tibial midshaft, with and without softtissue signal suppression. A, Gradient-echo (GRE) image. B, Radial ultrashort echo-time images. C, Radial ultrashort echo-time images with soft-tissue suppression (suppr.). Circular structure is the reference sample with T2 at approximately 300 μsec which, similar to bone, is visible only on radial MR images. Reproduced in part from (139).

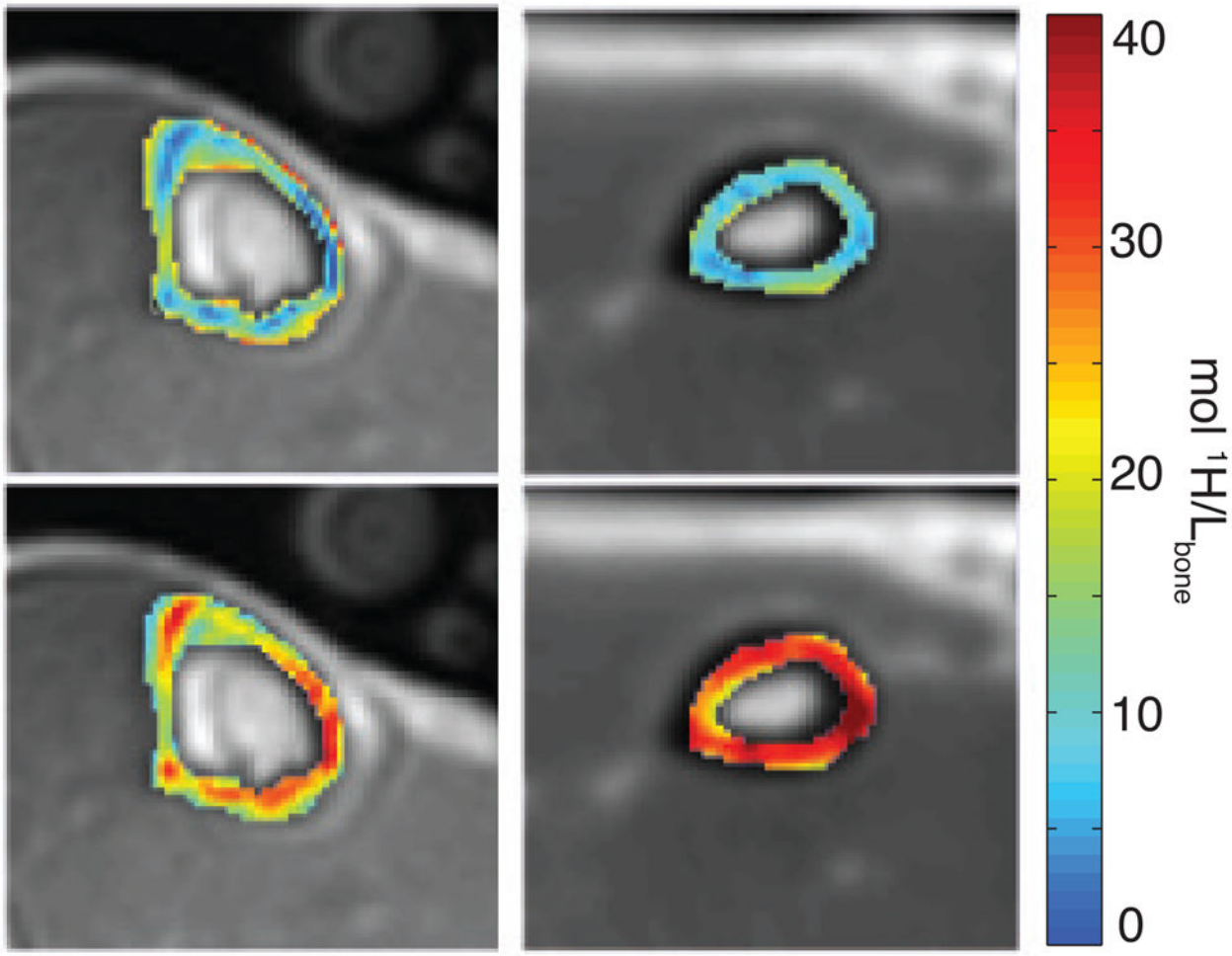

Figure 6.

Axial MR images obtained in vivo in the lower leg (left) and wrist (right) in a healthy subject; images are conventional UTE images overlaid with pore (top row) and bound (bottom row) water maps in the tibia and the radius. Reproduced in part from (143). 45

Table 1

Summary of imaging modalities with respect to advantages, disadvantages, and characteristics assessed

Imaging Method	Ionizing Radiation	Cost/ Time	Structural Characteristics	Material Characteristics	Associated Tools
DXA	low	low	—	aBMD	TBS, risk factor models[+]
QCT	high	high	macro-structure	vBMD	FEA
HR-pQCT	low[*]	high	macro-structure, porosity, trabecular architecture	vBMD	μFEA
QUS	none	low	—	SoS, BUA	QUI, SI
μMRI	none	high	macro-structure, trabecular architecture	—	μFEA
Marrow MRI	none	high	—	fat fractions	—
Bound/Pore Water MRI	none	high	macro-structure	bound water, pore water	—

[*] limited to extremities to maintain low dose

[+] These tools (e.g. FRAX, Garvan, QFracture) have only been used with DXA, but could potentially be applied to other imaging modalities.